Adsorption properties of polyacrylamide/*Nicandra physaloides* (L.) *gaertn* gel to Congo red

Wenshuo Xu[a], Yanhui Li[a,b,*], Meixiu Li[b], Huimin Wang[a], Yong Sun[a], Mingfei Cui[a], Liubo Li[a]

[a]*State Key Laboratory of Bio-fibers and Eco-textiles, College of Mechanical and Electrical Engineering, Qingdao University, Qingdao 266071, China, Tel. +86-532-85951842; email: liyanhui537@163.com (Y. Li)*
[b]*College of Materials Science and Engineering, Qingdao University, 308 Ningxia Road, Qingdao 266071, China*

ABSTRACT

In this paper, a facile freeze-drying method was used to prepare composites polyacrylamide/*Nicandra physaloides* (L.) *gaertn* seed gum (PAM/NPG), and it showed high adsorption properties to Congo red (CR) in the aqueous solution. The properties of the materials were investigated by scanning electron microscopy (SEM), Fourier-transform infrared spectroscopy, specific surface area analysis (BET) and thermogravimetric analysis. The adsorption properties of CR were investigated at different temperature, contact time, dosage of adsorption, pH, and initial concentration. The experimental results show that the maximum removal of CR from PAM/NPG aerogel is 684.931 mg/g when the temperature is 298 K and pH is 6. The pseudo-first-order kinetic model and Freundlich isothermal model are the best model to describe the adsorption behavior and the adsorption process is exothermic and spontaneous.

Keywords: Adsorption; Polyacrylamide; Congo red; *Nicandra physaloides* (L.) *gaertn* seed gum; Kinetic; Thermodynamic

1. Introduction

Nowadays, various organic dyes are well established in the textile printing and dyeing industry, papermaking, cosmetics, leather color photography, etc. The printing and dyeing industry produces large quantities of dyes [1]. Most of these are aromatic, polycyclic aromatic hydrocarbons and heterocyclic compounds. If these dyes are discharged directly into the water environment, the treatment of organic wastewater will be extremely difficult [2]. These dyes will prevent the sunlight from penetrating the water body, impair the photosynthesis and affect the healthy growth of aquatic organisms [3]. When organic dyes are decomposed in water, they will consume a large amount of oxygen, resulting in anoxic water, its characteristics are that water has odor and decay, [4] which is not conducive

to the growth of aquatic animals and plants, and seriously pollutes the scarce freshwater resources [5]. Some azo dyes are carcinogenic and will cause great harm to people's living environment and health. For example, Congo red (CR) [6] is one of the most difficult dyes to remove. Das et al. [7] offered the adsorption performance of nanocomposite for CR in aqueous solution. Therefore, seeking an effective method to remove CR in wastewater has attracted more and more attention [8].

At present, dye removal methods include photocatalytic biological oxidation [9], degradation [10], adsorption [11,12], chemical precipitation [13], membrane filtration [14] and ion exchange [15]. Compared with other methods, adsorption is a low-cost and simple method, which can effectively remove dyes from waste liquid [16]. Various adsorbents can be used for wastewater treatment, such as activated carbon [17], zeolite [18], carbon nanotubes [19],

* Corresponding author.

graphene [20] and synthetic materials [21,22]. However, most of the adsorbents cannot be widely used in water due to the high cost [23]. In recent years, a variety of synthetic adsorbents [24] have been widely used in wastewater adsorption due to their low cost, easy availability and eco-friendly. With the rapid development of organic polymer technology, many modified materials [25] have high specific surface area, strong mechanical stability and good regeneration performance [26].

Polyacrylamide (PAM) is an organic polymer material. Because its amide group unit [27], it can form hydrogen bond with sulfonic acid group or phenolic hydroxyl group in synthetic pigment, so it has adsorption effect on synthetic pigment [28]. The effect of pure PAM as adsorbent is not good [29], therefore, chemical, or physical methods can change the properties of experimental materials [30]. The physical modification is to mix with other substances through the internal force of hydrogen bond and van der Waals force, without chemical reaction [31]. By contrast, grafting [32,33], copolymerization and crosslinking [34,35] are the most commonly used techniques to modifying PAM. The modified PAM has strong adsorption capacity and can separate dyes and heavy metal ions from aqueous solution. Modified PAM can also be used in petroleum production [36,37], oil–water separation, leather and coating [38]. PAM and its complexes are widely used in the treatment of dye wastewater due to their excellent properties.

Nicandra physaloides (L.) *gaertn* seed gum (NPG) is a kind of low-cost polysaccharide; it was isolated from the *Nicandra physaloides* (L.) *gaertn* seed colloid by distilled water extraction. Mainly composed of galacturonic acid, glucose, galactose, and rhamnose [39]. When forming a gel, the spherical molecules of NPG are connected end to end to form a chain structure with branch nodes [40]. The network structure is further chelated with other substances to form a porous network [41].

In this paper, based on the above exemplar properties of PAM and NPG, a novel PAM and NPG polymer adsorbent polyacrylamide/*Nicandra physaloides* (L.) *gaertn* seed gum (PAM/NPG) for removing CR was prepared by grafting polyacrylamide onto NPG substrate under the action of initiator. This paper studies and compares the characteristics of PAM, NPG, and PAM/NPG in detail. And the adsorption behavior of PAM/NPG on CR wastewater was studied. The effects of temperature, pH, temperature, contact time and adsorbent dose on the adsorption performance were further studied by batch adsorption experiments. Determine the most suitable isotherm, thermodynamic and kinetic model.

2. Materials and methods

2.1. Material

CR ($C_{32}H_{22}N_6Na_2O_6S_2$, purity >99%) and anhydrous ethanol was bought from Tianjin Dengke Chemical Reagent Co., Ltd., acrylamide (AM) and Na_2SO_3 were purchased from Tianjin Guangfu Fine Chemical Industry Co., Ltd., ammonium persulfate (APS) and N,N′-methylene-bis(acrylamide)(MBA) were purchased from Sinopharm Chemical Reagent Co., Ltd., NPG was provided by Sichuan

Gurunangsheng, and deionized water was used for solution preparation. The other chemical reagents used in this experiment were bought from Sinopharm Chemical Reagent Co., Ltd., and they are all analytically pure without further purification.

2.2. Preparation of NPG

At a temperature of 298 K, 30 g NPG seeds were weighed and rinsed simply rinse with deionized water to remove surface impurities. Then put the seeds into 250 mL deionized water, the seeds were ultrasonically vibrated for 5 min, and then stirred for 2 min, filter out the seeds to obtain the filtrate, repeat this step several times, the obtained filtrate was frozen, and put it in a freeze dryer to obtain NPG glue.

2.3. Preparation of PAM/NPG

PAM/NPG was synthesized by crosslinking in the presence of initiator. Dissolve 5 g AM in 30 mL distilled water, stir until it is completely dissolved, add 0.2 g MBA and 0.15 g Na_2SO_3, and dissolve 0.25 g APS in 13 mL deionized water. Continue stirring for 2 h under the bubbling condition of nitrogen, which acts as deoxygenation, and then set aside. Dissolve 0.2 g PNG glue in 10 mL of distilled water to prepare NPG solutions. PAM were added to the PNG solutions, and stir the mixture continuously until uniform. Finally, the mixture was heated at 333 K for 20 min to obtain the composite material gel, which was repeatedly washed with anhydrous ethanol and distilled water and purified. The obtained material was frozen and put into a freeze-drying machine to obtain gel. Pure polyacrylamide is the same as the above method, but without adding PNG solution.

2.4. Characterization of PAM/NPG

The surface morphologies of PAM/NPG fibers were characterized by the scanning electron microscopy (SEM TM-3000, HitachiSU-70, Japan). Fourier-transform infrared spectroscopy (FTIR Nicolet iS10, Thermo Scientific, USA) was measured to analyze the surface functional groups of the sample. Thermal degradation analysis (TGA, Perkin Elmer, ASTA 6000) was used to analyze thermal stability of PAM/NPG at the heating rate of 10 K/min and temperature of 303 to 1,073 K. The samples were vacuum dried and the specific surface area and pore size distribution was obtained at 77 K through the N_2 adsorption isotherm (BET Micromeritics ASAP2460-2 M, Mike, USA).

2.5. Adsorption experiment

All adsorption experiments were performed in water bath temperature-controlled oscillator. Dissolve 0.5 g CR in 500 mL flask and prepare 1,000 mg/L CR. In the experiment, different concentrations of CR solution were diluted from the original solution. Then the conical flask was placed in a constant temperature gas bath oscillator and stirred at a speed of 160 rpm for 48 h to achieve adsorption equilibrium. Check the equilibrium concentration of

chromium with an UV-Vis spectrophotometer. The adsorption capacity of the composite [42] can be obtained by Eq. (1)

$$q_e = \left(\frac{C_0 - C_e}{m} \right) V \qquad (1)$$

where the equilibrium concentration is expressed by C_e (mg/L), C_0 (mg/L) is the initial concentration of CR solution, the solution mass is m (g), and the volume of adsorbent used is V (L).

Different doses of PAM/NPG (5, 10, 15, 20, 25, 30 mg) were added into 20 mL CR solution (100 mg/L) to realize the effect of adsorbent dosage on adsorption. Add 10 mg composites to 20 mL chromium solution (100 mg/L) and study how pH affects adsorption by changing the pH range (4–10). The effect of contact time was evaluated by putting 125 mg composite into 250 mL CR solution (100 mg/L) to measure the concentration of CR at different contact times. The effect of temperature was researched in CR solution at different concentrations (40~140 mg/L). Eq. (2) is the adsorption quantity q_t formula [43]:

$$q_t = \left(\frac{C_0 - C_t}{m} \right) V \qquad (2)$$

The mass of adsorbent is expressed by m (g). The concentration of CR at t time is C_t (mg/g), and the volume of solution is V (L).

3. Results and discussion

3.1. Characterization of adsorbent

The electron micrograph of pure NPG is shown in Fig. 1a and b. The results showed that the surface of NPG is dense and smooth with no visible pores and few
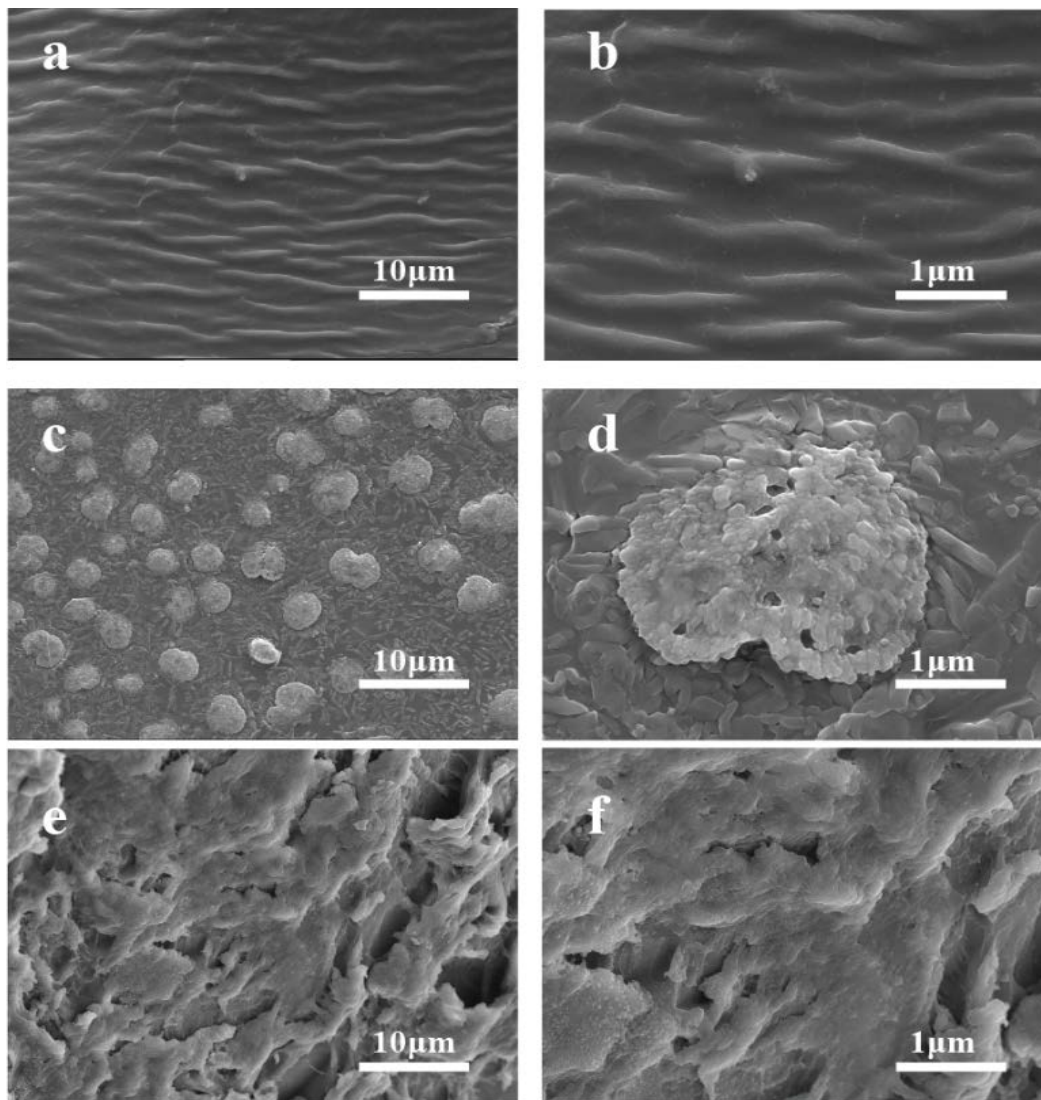

Fig. 1. (a and b) Shows the structure of pure NPG under scanning electron microscope. (c and d) is the structure diagram of pure PAM under scanning electron microscope. (e and f) is structure diagram under SEM images of PAM/NPG.

wrinkles. Fig. 1c and d is the pure PAM material. It can be observed that the surface is less rough and there are only a few gullies in the aerogel, indicating that the aerogel possesses a small specific surface area and almost no pore structure. Fig. 1e and f show that the material has a porous, non-uniform surface, adding more folds. The results show that cross-linking makes the specific surface area of the composite material larger and rougher, so that the composite material has a highly developed pore structure, the specific surface area and porosity, and make CR molecules more easily diffuse into the composite, so as to make the adsorption process easier and obtain higher adsorption capacity and efficiency. The results shows that PAM/NPG is successfully formed.

The FTIR spectrum in Fig. 2 provides evidence for the presence of PAM and NPG in the frozen gel forming an interpenetrating network. It can be seen from curve a that the –OH stretching vibration causes gel produce a strong peak at 3,446 cm^{-1} [44], and the absorption peak at 2,924 cm^{-1} is caused by the C–H stretching vibration. The asymmetric stretching vibration and symmetric stretching vibration of the carboxylate anion have absorption peaks at 1,635 and 1,402 cm^{-1} [45], respectively. The weak peak at 1,240 cm^{-1} is the C–O–C stretching vibration peak of asymmetric polysaccharide. Curve b shows that 3,453 cm^{-1} is the characteristic absorption peak of –NH$_2$, 2,925 cm^{-1} is the characteristic absorption peak of methylene antisymmetric stretching vibration, 2,860 cm^{-1} is the characteristic absorption peak of methylene symmetric stretching vibration, 1,631 cm^{-1} is the characteristic absorption peak of carbonyl group, corresponding to amide group (C=O stretching vibration) [46], 1,405 cm^{-1} is the characteristic absorption peak of methylene deformation. It can be seen from curve c that PAM/NPG has absorption peaks of NPG and PAM, indicating that NPG and PAM are well synthesized.

Fig. 3 shows the thermogravimetric analysis curves of PAM/NPG composites, pure NPG, and pure PAM. The weight loss of NPG and PAM/NPG is evident in the first stage (T1–T2), which is caused by evaporation water
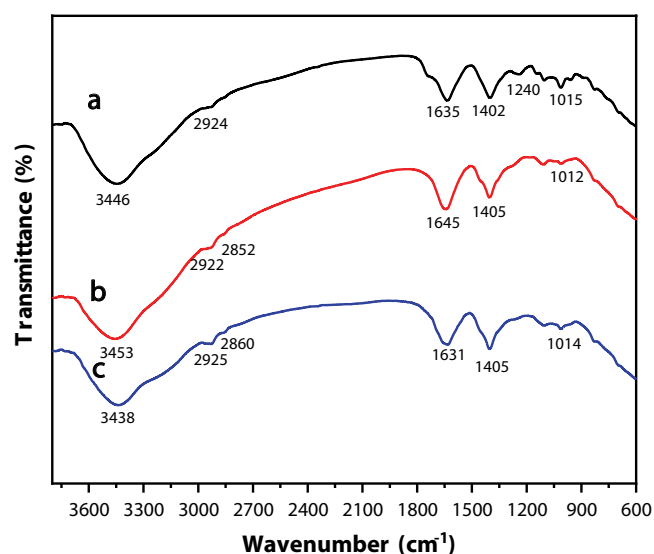
molecules attached to the hydrophilic group. The next stage of NPG is caused by the decomposition of the material, while the second stage (T2–T3) of PAM/NPG is caused by the fracture of the material and the fracture of the main chain and the initiation of the amide. The main weight loss of PAM is water loss and the material decomposition. The final residual weight of the composite material is 50% of the original weight, which is significantly higher than the 30% and 20% of the pure material. It can be seen that the weight loss of the composite material is less than that of the two pure materials, indicating that the homemade PAM/NPG composite material has better thermal stability.

The specific surface area and pore size distribution of PAM/NPG were measured by BET. Fig. 4a is N$_2$ adsorption-desorption isotherms of NPG and PAM/NPG. The BET specific surface area of PAM/NPG was 4.4464 m^2/g. It was significantly higher than 0.7123 m^2/g of NPG. In addition, the pore size distribution of PAM/NPG composites can be seen from the Fig. 4b. The pore size distribution of PAM/NPG adsorbent is 25 ~ 35 Å, which confirms the mesoporous properties of the material.

3.2. Effect of contact time

The effect of contact time in CR is shown in Fig. 5. The slope of the curve decreases obviously, indicating that the adsorption rate also decreases with the decrease of time and means that the adsorption effect is gradually weakened. Adsorption reaches equilibrium after about 1,200 min. This has been reported before. The specific reason may be that the active site is occupied by CR over time. At the beginning of the adsorption process, more active sites contact and combine with CR on the surface of adsorbent, resulting in a rapid reduction of CR in the solution [47]. With the passage of time, the active center gradually decreased, which makes the adsorption process slow down gradually and finally reaches the adsorption equilibrium [48].
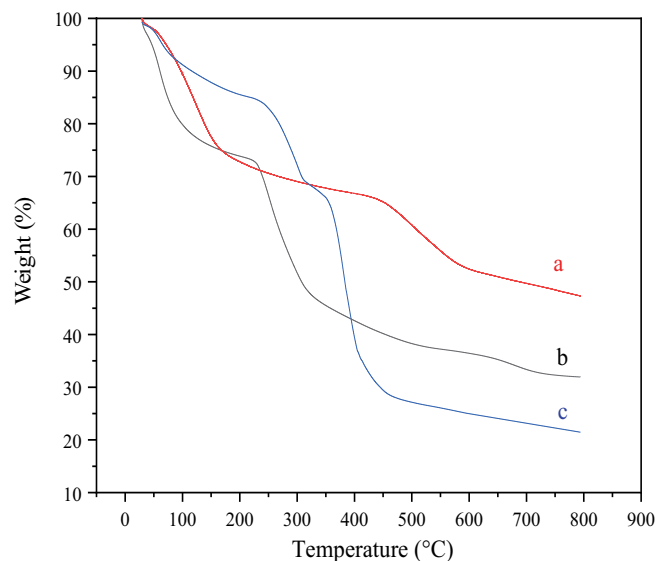

Fig. 2. FTIR spectra of (a) NPG, (b) PAM, and (c) PAM/NPG.

Fig. 3. TGA curves of (a) PAM/NPG, (b) NPG, and (c) PAM.

3.3. pH effect

The pH value of dye reagent is also an important criterion for evaluating adsorption performance [49]. Adjust the CR solution from 3 to 10 with acid and alkali, and then the adsorbent was tested (Fig. 5b), the results displayed the adsorption capacity of CR solution was higher when the pH is 4–6. The removal rate of CR was over 90%. When the pH value is 6, the removal rate reaches the maximum value (94.244%). When the pH value is higher than 6, the adsorption capacity gradually decreases and the CR removal rate

decreases. Theoretically, pH affects the surface charges, and dissociation of pollutant molecules and functional groups does exist. In acid solution, the carboxyl group of adsorbent binds to CR molecule at acidic pH. Oxygen-containing functional groups have a great influence on the whole adsorption process. At acidic pH, CR molecules are a cationic and can be linked to the carboxyl group of adsorbent [50]. In the alkaline pH, CR molecule is anionic, and the carboxyl functional group of the adsorbent is also converted into anionic properties, and the adsorbent cannot be combined with dye molecules to achieve adsorption purpose. At the
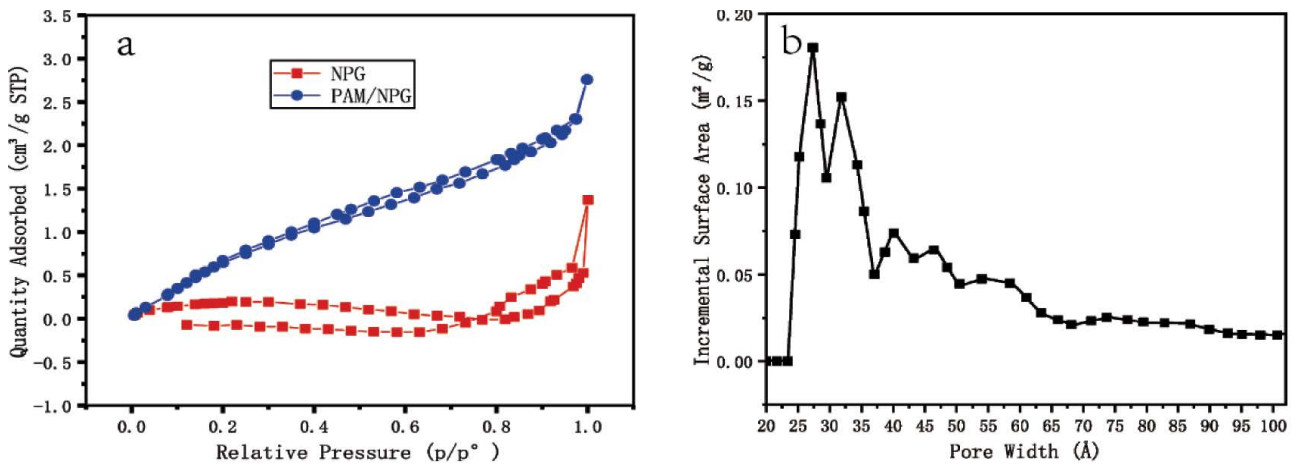

Fig. 4. (a) N_2 adsorption–desorption isotherms of NPG and PAM/NPG and (b) pore size distribution of PAM/NPG.
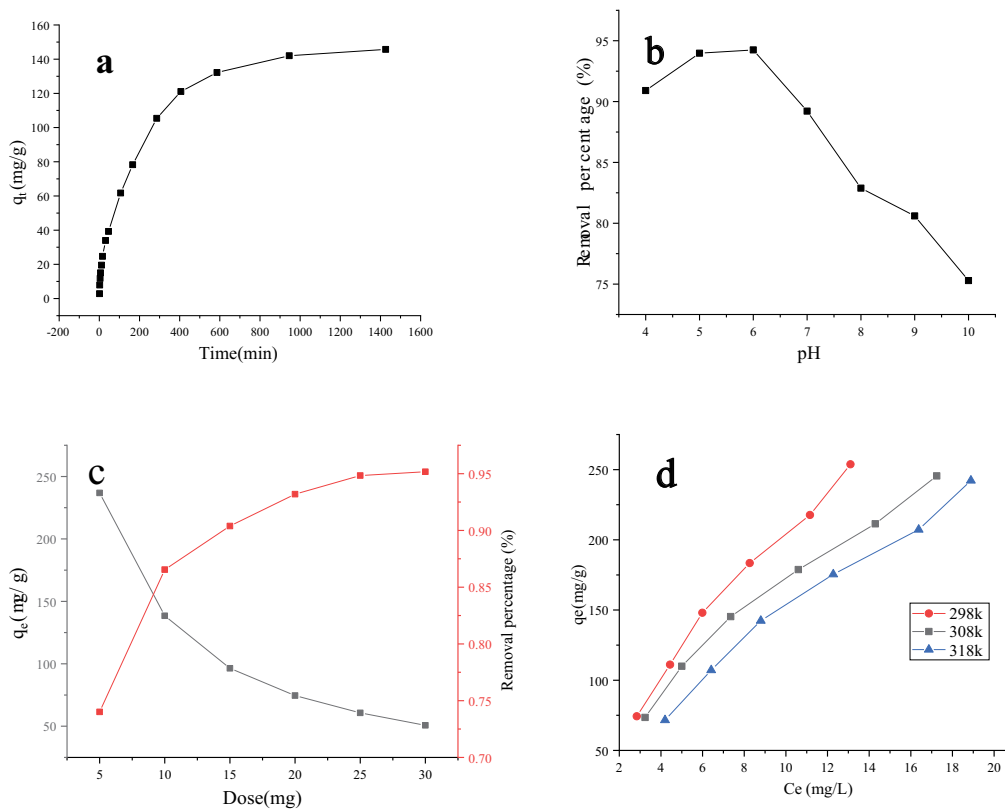

Fig. 5. Effect of different experimental parameters on CR on PAM/NPG: (a) contact time, (b) pH, (c) dose, and (d) temperature.

same time, the strength and adsorption sites of NPG seed gum decreased under alkaline conditions. All of these lead to the decrease of CR removal rate at higher pH [51].

3.4. Effect of adsorbent dosage

One of the key parameters affecting adsorption results is the amount of adsorbent. Fig. 5c shows the removal results of different doses. When the dosage of adsorbent increased from 5 to 20 mg, the removal rate of CR increased significantly. This is because with the increase of the amount of adsorbent, the specific surface area and adsorption site increase, resulting in an increase in removal rate [52]. However, as the dose continues to increase to above 20 mg, the amount of adsorption did not increase significantly, there was no significant increase in adsorption capacity, possibly because CR did not occupy all active sites [53].

3.5. Effect of temperature

Temperature is the key link in the whole adsorption process. The impregnation process at 298, 308 and 318 K conditions was studied respectively (Fig. 5d). The results show that when the initial concentration is 80 mg/L, the increase of temperature will lead to the decrease of adsorption effect. When the temperature was 298 K, the adsorption capacity was 253.796 mg/g, and when the temperature increased to 318 K, the adsorption capacity decreased to 242.226 mg/g. The higher the temperature, the lower the adsorption capacity, which maybe due to the inhibition of hydrogen bond between functional groups

and dye molecules [54]. In conclusion, the adsorption process is exothermic.

3.6. Adsorption isotherm

The adsorption isotherm gives a good indication of the adsorption capacity. Langmuir and Freundlich compliant adsorption isotherm are the two recognized adsorption isotherm models.

Langmuir model suggests that the adsorption occurs on a homogeneous surface and the whole process is monolayer. The Langmuir equation (Fig. 6a) is as follows [55]:

$$\frac{C_e}{q_e} = \frac{C_e}{q_{max}} + \frac{1}{q_{max}k_L} \tag{3}$$

where the equilibrium concentration and equilibrium adsorption capacity are C_e (mg/L) and q_e (mg/g) respectively, q_{max} (mg/g) represents the maximum adsorption capacity, and the Langmuir constant is represented by k_L (L/g), q_{max} and k_L can be obtained from the intercept and slope of linear function respectively, as shown in Table 1. The isotherm indicates a maximum sorption of 684.931 mg/g for PAM/NPG, which was higher than pure NPG. If the coefficient R^2 is higher, then the adsorption process is closer to the Langmuir model. Another dimensionless parameter of Langmuir model is R_L, which is obtained by [56]:

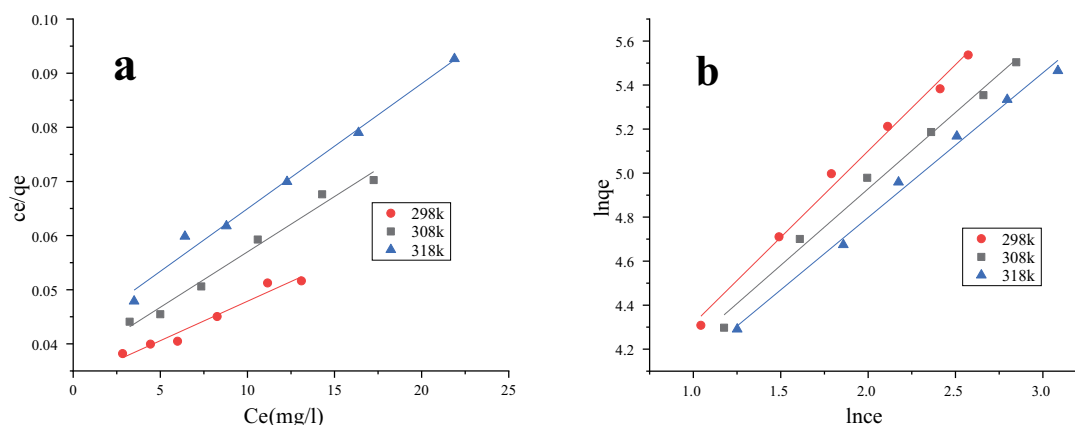$$R_L = \frac{1}{1 + C_0 k_L} \tag{4}$$

Fig. 6. Equilibrium isotherms of CR on PAM/NPG at 298, 308 and 318 K: (a) the Langmuir isotherm, and (b) the Freundlich isotherm.

Table 1
Adsorption isotherm model parameters of PAM/NPG adsorbed CR

T (K)	Langmuir				Freundlich		
	q_{max} (mg/g)	k_L (L/mg)	R^2	R_L	1/n	R^2	k_F (L/mg)
298	684.931	0.04383	0.9621	0.141–0.363	0.784	0.9923	34.158
308	487.805	0.05612	0.9834	0.113–0.308	0.694	0.9904	34.422
318	432.901	0.05521	0.9878	0.114–0.317	0.657	0.9928	32.554

Langmuir isotherms can be favorable, unfavorable, irreversible, and linear. These can be reflected in the data R_L, as shown in Table 1. The R_L value is between 0 and 1, indicating that the composite absorbs CR well.

The Freundlich model is designed to allow for multilayer adsorption and to occur on heterogeneous surfaces. The Freundlich model (Fig. 6b) is formulated as follows [57].

$$\ln q_e = \ln k_F + \frac{1}{n} \ln C_e \qquad (5)$$

where k_F (L/mg) is a capacity parameter reflecting adsorption, and n is an empirical parameter reflecting the strength of the adsorption. It is obtained from the intercept and slope of Fig. 6b respectively. As shown in Table 1, n always greater than 1, which proving that the adsorption process is prone to occurs, which also corresponds to the previous equation. As can be seen from Table 1 that the R^2 value for the Freundlich equation is greater than that for the Langmuir equation. Therefore, the adsorption of CR on composite materials is more consistent with Freundlich isothermal adsorption model. That is, PAM/NPG adsorbed on heterogeneous adsorption sites, which different adsorption energies.

Reports on the use of other materials for the remove of CR from aqueous solutions are shown in Table 2. PAM/NPG has a higher adsorption capacity for CR and is more effective than other adsorbents.

3.7. Kinetic studies

There are three widely accepted kinetic models to simulate the adsorption process: pseudo-first-order kinetic model, pseudo-second-order kinetic model and intra-particle diffusion model.

The following describes the pseudo-first-order equation [64]:

$$\log(q_e - q_t) = \log q_e - \frac{k_1}{2.303}t \qquad (6)$$

The following describes the pseudo-second-order equation [65]:

$$\frac{t}{q_t} = \frac{1}{k_2 q_e^2} + \frac{t}{q_e} \qquad (7)$$

The adsorption capacity at time t and equilibrium time are expressed by q_t and q_e (mg/g) respectively. The rate constant for the pseudo-first-order kinetic model (Fig. 7a) and the rate constant for the pseudo-second-order kinetic model (Fig. 7b) are expressed as k_1 (1/min) and k_2 (1/min), respectively. After linear fitting, k_1 and q_e are obtained from slope and k_2 from intercept (Table 3). The results indicate that the adsorption process is more suitable for the pseudo-first-order kinetic model. Furthermore, the obtained q_e agrees with the experimental data, which also confirms that the experiment is closer to the pseudo-first-order model.

The purpose of introducing the intraparticle diffusion model is to investigate the principle of CR diffusion in the composite. According to Weber and Morris theory derived from experience, the adsorption capacity is proportional to 1/2, and the equation is as follows [66]:

$$q_t = k_{id} t^{1/2} + C_i \qquad (8)$$

where C_i is the I intercept and is strongly influenced by the boundary layer. The intra particle diffusion constant is expressed as k_{id} (mg/g min$^{1/2}$). The k_{id} and C_i are obtained from intercept and slope by linear fitting. Fig. 7c indicates that the adsorption process can be divided into two parts. In the first stage, more active sites can be seen binding to CR on the surface of the adsorbent. After the second stage, the adsorption rate gradually slows down, indicating that the adsorption within the adsorbent has become dominant.

3.8. Thermodynamic study

Thermodynamic analysis of Gibbs free energy (ΔG), enthalpy (ΔH), and entropy (ΔS) was carried at 298, 308, and 318 K temperatures. The thermodynamic equations are (1) [67]:

$$\Delta G = \Delta H - T\Delta S \qquad (9)$$

$$\ln\left(\frac{q_e}{C_e}\right) = -\frac{\Delta H}{RT} + \frac{\Delta S}{R} \qquad (10)$$

Table 2
Comparison of different adsorbents to remove CR

| Adsorbents	Adsorbate	q_m (mg/g)	Reference
PAM/NPG	Congo red	684.931	This study
HDTMA modified clinoptilolite	Congo red	200	[58]
Hydrothermal treated shiitake mushroom	Congo red	217.86	[59]
Citric acid incorporated bentonite	Congo red	384	[60]
Improved gluten material	Congo red	211.1	[5]
MgO/Calcium alginate	Congo red	344.8	[61]
Egg shell membrane (ESM)	Congo red	117.65	[62]
Porous γ-alumina nanoshells	Congo red	370.4	[63]
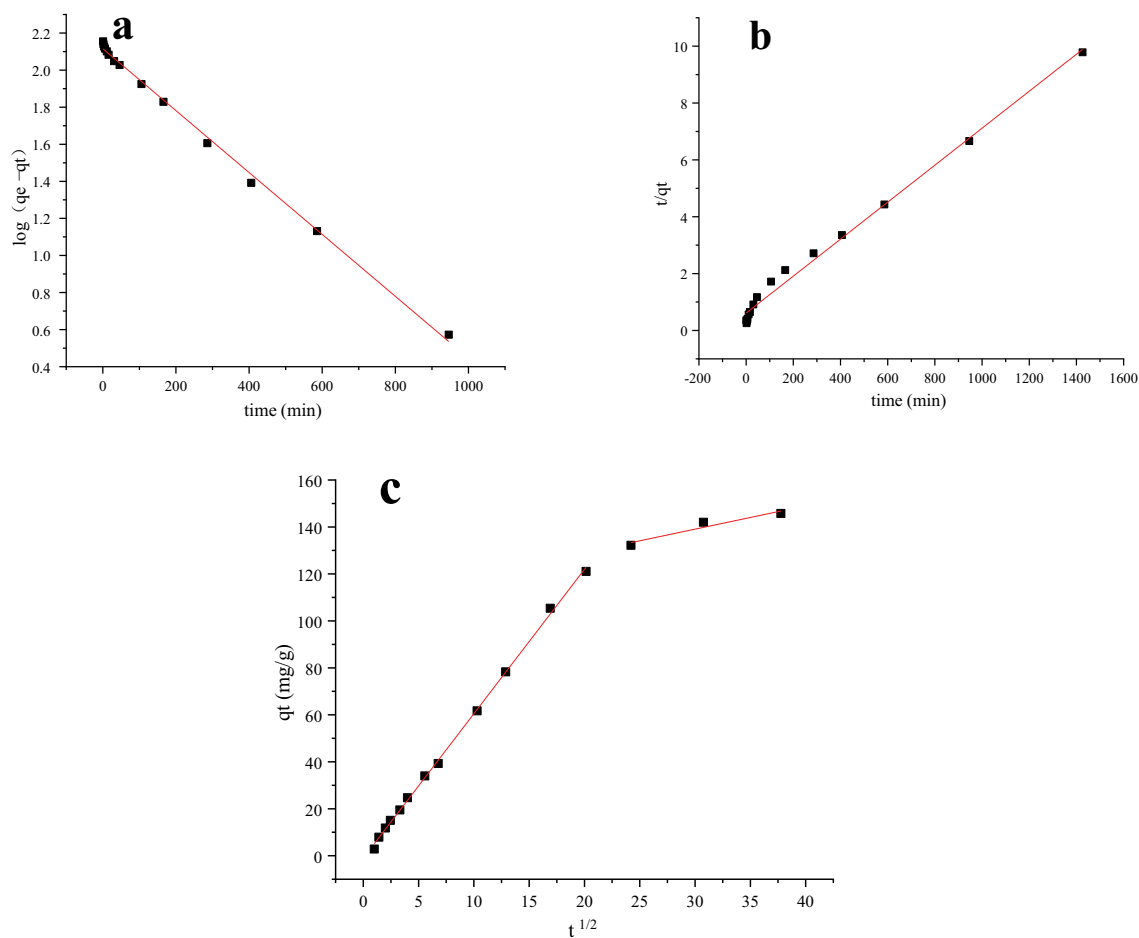
Fig. 7. Adsorption kinetics of CR adsorbed by PAM/NPG: (a) pseudo-first-order model, (b) pseudo-second-order model, and (c) intraparticle diffusion model.

Table 3
Kinetic constants of adsorption of CR onto PAM/NPG

Kinetic model	Parameters	Values
	k_1 (min^{-1})	3.85×10^{-3}
Pseudo-first-order	q_e (mg/g)	130.431
	R^2	0.99723
	k_2 (g/mg min)	6.94×10^{-5}
Pseudo-second-order	q_e (mg/g)	153.609
	R^2	0.99142
	k_{id1} (mg/g min$^{1/2}$)	6.147
	C_1 (mg/g)	−1
	R_1^2	0.9988
Intraparticle diffusion model	k_{id2} (mg/g min$^{1/2}$)	0.99
	C_2 (mg/g)	109.28
	R_2^2	0.9275

The general gas constant can be expressed as R (8.314 kJ/mol). ΔS and ΔH are calculated by intercepting and gradienting the $1/T$ curve of $\ln(q_e/C_e)$.

As shown in Table 4 ΔG = 7.9 kJ/mol indicates that the adsorption process is spontaneous and feasible. The

Table 4
Thermodynamic parameters for CR adsorbed by PAM/NPG

T/K	ΔG (kJ/mol)	ΔH (kJ/mol)	ΔS (J/mol K)
298	−7.941	−16.667	−29.28
308	−7.648		
318	−7.355		

negative enthalpy change (ΔH = 16.667 kJ/mol) indicates that the adsorption process is exothermic. The negative entropy change (ΔS = 29.2 J/mol) indicates that the adsorption disorder random interface reduced.

3.9. Adsorption mechanism

The preparation and adsorption mechanism of PAM/NPG aerogels are shown in Fig. 8. The high adsorption capacity of PAM/NPG aerogel for Congo red dye is mainly due to the porous structure and the binding of adsorption functional groups. The organic polymer chains and chemical groups can easily bind to the Congo red molecule. And its own charge is easily attracted to the Congo red molecule by electrostatic gravity. The Congo red molecule also
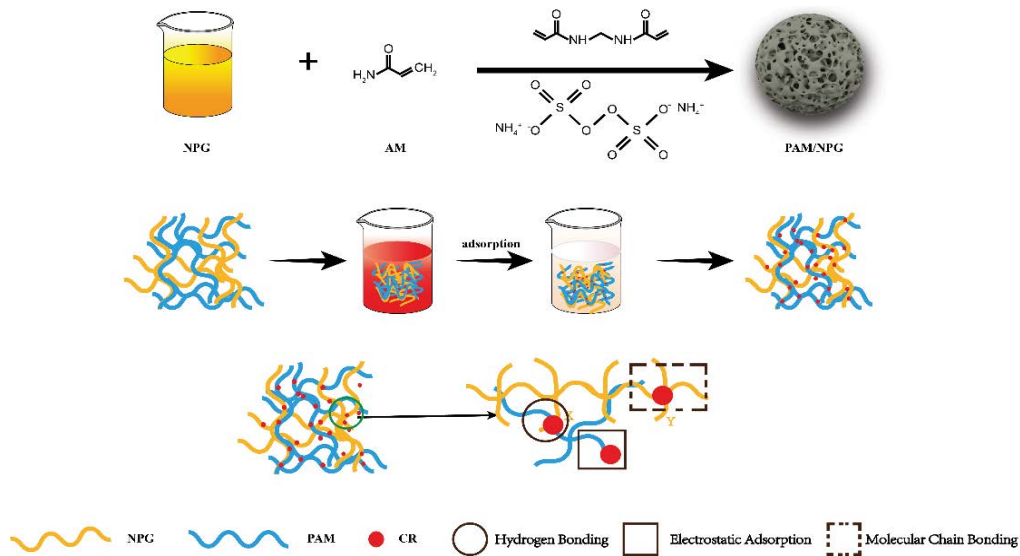
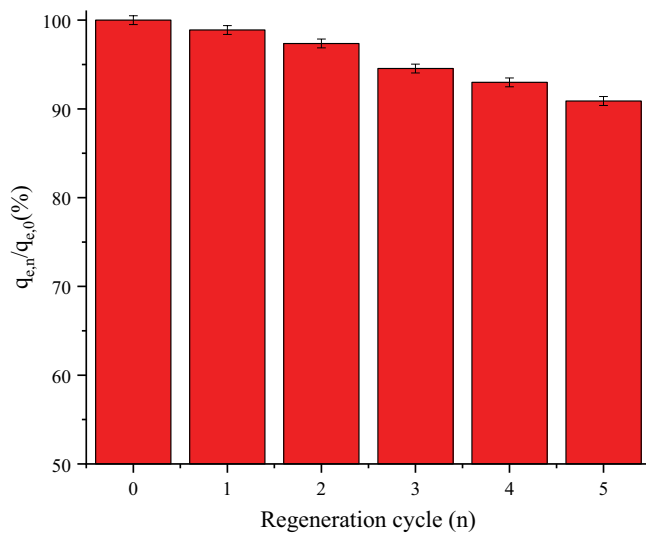Fig. 8. Preparation process and adsorption mechanism of PAM/NPG.

Fig. 9. Regeneration performance of PAM/NPG.

easily interacts with the polar groups of PAM/NPG (mono CH$_2$ mono CHCO mono) through hydrogen bonding [68].

3.10. Regeneration characteristics

The regeneration ability of the adsorbent is of great interest. Desorption experiments were carried out by placing 20 mg of adsorbent that had reached adsorption equilibrium into a solution of HCl at a concentration of 0.3 M to ensure that desorption was complete. The relative ratio of adsorption capacity was calculated for each cycle using $q_{e,n}/q_{e,0}$, where n is the number of cycles, and the results are shown in Fig. 9. The relative adsorption capacity exceeded 90% after 5 cycles, indicating that the adsorbent has good performance in terms of recovery and regeneration capacity.

4. Conclusion

A novel of low cost biosorbent was prepared by simple crosslinking reaction. The surface morphology, functional groups and thermal stability of the adsorbent were investigated by SEM, FTIR and TGA. The effects of the amount of adsorbent, temperature, contact time and pH on CR adsorption are discussed. The results show that the optimum pH is 6 and the optimum temperature is 298 K. The maximum adsorption capacity of the adsorbent toward CR is 684.931 mg/g. The pseudo-first-order kinetic model is more suitable to describe the adsorption of chromium by the adsorbent, and another Freundlich isothermal model is also more suitable to describe the process. By thermodynamic analysis, the adsorption process of PAM/NPG on the dye is spontaneous and exothermic. The experimental results show that the PAM/NPG can effectively remove CR in water. The results indicate that the composite has a good prospect for CR adsorption. The results show that PAM/NPG biomodifier can effectively remove CR from water.

Declaration of interest statement

The authors declare that they have no known competing financial interests or personal relationships that could have appeared to influence the work reported in this paper.

References

[1] G. Crini, Non-conventional low-cost adsorbents for dye removal: a review, Bioresour. Technol., 97 (2006) 1061–1085.
[2] M.I. Khan, S. Akhtar, S. Zafar, A. Shaheen, M.A. Khan, R. Luque, A. ur Rehman, Removal of Congo red from aqueous solution by

anion exchange membrane (EBTAC): adsorption kinetics and themodynamics, Materials, 8 (2015) 4147–4161.

[3] X.P. Zhang, Y.H. Li, M.X. Li, H. Zheng, Q.J. Du, H. Li, Y.Q. Wang, D.C. Wang, C.P. Wang, K.Y. Sui, H.L. Li, Y.Z. Xia, Removal of methylene blue from aqueous solution using high performance calcium alginate/activated carbon membrane, Int. J. Clothing Sci. Technol., 32 (2020) 307–321.

[4] K. Tang, Y. Li, X. Zhang, M. Li, Q. Du, H. Li, Y. Wang, D. Wang, C. Wang, K. Sui, H. Li, Y. Xia, Synthesis of citric acid modified β-cyclodextrin/activated carbon hybrid composite and their adsorption properties toward methylene blue, J. Appl. Polym. Sci., 137 (2020) 48315, doi: 10.1002/app.48315.

[5] X. Zhang, Y. Li, M. Li, H. Zheng, Q. Du, H. Li, Y. Wang, D. Wang, C. Wang, K. Sui, H. Li, Y. Xia, Preparation of improved gluten material and its adsorption behavior for Congo red from aqueous solution, J. Colloid Interface Sci., 556 (2019) 249–257.

[6] C. Jeyaseelan, N. Chaudhary, R. Jugade, Sulphate-crosslinked chitosan as an adsorbent for the removal of Congo red dye from aqueous solution, Air Soil Water Res., 11 (2018), doi: 10.1177/1178622118811680.

[7] P. Das, A. Debnath, B. Saha, Ultrasound-assisted enhanced and rapid uptake of anionic dyes from the binary system onto $MnFe_2O_4$/polyaniline nanocomposite at neutral pH, Appl. Organomet. Chem., 34 (2020) e5711, doi: 10.1002/aoc.5711.

[8] M.F. Cui, Y.H. Li, Y. Sun, H.M. Wang, M.X. Li, L.B. Li, W.S. Xu, Study on adsorption performance of MgO/calcium alginate composite for Congo red in wastewater, J. Polym. Environ., 29 (2021), doi: 10.1007/s10924-021-02170-x.

[9] D.R. Manenti, A.N. Modenes, P.A. Soares, F.R. Espinoza-Quinones, R.A.R. Boaventura, R. Bergamasco, V.J.P. Vilar, Assessment of a multistage system based on electrocoagulation, solar photo-Fenton and biological oxidation processes for real textile wastewater treatment, Chem. Eng. J., 252 (2014) 120–130.

[10] X.S. Wang, J.P. Chen, Biosorption of Congo red from aqueous solution using wheat bran and rice bran: batch studies, Sep. Sci. Technol., 44 (2009) 1452–1466.

[11] T. Zhao, Y. Yao, D.R. Li, F. Wu, C.Z. Zhang, B. Gao, Facile low-temperature one-step synthesis of pomelo peel biochar under air atmosphere and its adsorption behaviors for Ag(I) and Pb(II), Sci. Total Environ., 640 (2018) 73–79.

[12] P. Das, P. Debnath, A. Debnath, Enhanced sono-assisted adsorptive uptake of malachite green dye onto magnesium ferrite nanoparticles: kinetic, isotherm and cost analysis, Environ. Nanotechnol. Monit. Manage., 16 (2021) 100506, doi: 10.1016/j.enmm.2021.100506.

[13] Y.Q. Wang, Y.H. Li, X.P. Zhang, H. Zheng, Removal of Methylene blue from water by copper alginate/activated carbon aerogel: equilibrium, kinetic, and thermodynamic studies, J. Polym. Environ., 28 (2020) 200–210.

[14] X.C. Yan, X.P. Zhang, Q. Li, Preparation and characterization of CS/beta-CD/Nano-ZnO composite porous membrane optimized by Box–Behnken for the adsorption of Congo red, Environ. Sci. Pollut. Res., 25 (2018) 22244–22258.

[15] J. Labanda, J. Sabate, J. Llorens, Experimental and modeling study of the adsorption of single and binary dye solutions with an ion-exchange membrane adsorber, Chem. Eng. J., 166 (2011) 536–543.

[16] A. Azari, R. Nabizadeh, A.H. Mahvi, S. Nasseri, Magnetic multi-walled carbon nanotubes-loaded alginate for treatment of industrial dye manufacturing effluent: adsorption modelling and process optimisation by central composite face-central design, Int. J. Environ. Anal. Chem., (2021), doi: 10.1080/03067319.2021.1877279.

[17] N.A. Dahlan, S.L. Ng, J. Pushpamalar, Adsorption of methylene blue onto powdered activated carbon immobilized in a carboxymethyl sago pulp hydrogel, J. Appl. Polym. Sci., 134 (2017), doi: 10.1002/app.44271.

[18] M. Shaban, M.R. Abukhadra, M.G. Shahien, S.S. Ibrahim, Novel bentonite/zeolite-NaP composite efficiently removes methylene blue and Congo red dyes, Environ. Chem. Lett., 16 (2018) 275–280.

[19] E.S. Kastrisianaki-Guyton, L. Chen, S.E. Rogers, T. Cosgrove, J.S. van Duijneveldt, Adsorption of sodium dodecylsulfate on single-walled carbon nanotubes characterised using small-angle neutron scattering, J. Colloid Interface Sci., 472 (2016) 1–7.

[20] M.Z. Momcilovic, M.M. Purenovic, M.N. Miljkovic, A.L. Bojic, M.S. Randelovic, Adsorption of cationic dye Methylene blue onto activated carbon obtained from horse chestnut kernel, Hem Ind., 65 (2011) 123–129.

[21] B.B. Fang, Z.P. Bao, L. Lu, L.J. Zhao, H.Y. Wang, Preparation of a hierarchical flower-like γ-Al_2O_3@C composite exhibiting enhanced adsorption performance for Congo red by high temperature transformation of γ-AlOOH@C precursors, RSC Adv., 6 (2016) 61–64.

[22] P. Das, S. Nisa, A. Debnath, B. Saha, Enhanced adsorptive removal of toxic anionic dye by novel magnetic polymeric nanocomposite: optimization of process parameters, J. Dispersion Sci. Technol., (2020), doi: 10.1080/01932691.2020.1845958.

[23] K. Yang, Y.H. Li, H. Zheng, X.Y. Luan, H. Li, Y.Q. Wang, Q.J. Du, K.Y. Sui, H.L. Li, Y.Z. Xia, Adsorption of Congo red with hydrothermal treated shiitake mushroom, Mater. Res. Express, 7 (2020) 015103, doi: 10.1088/2053-1591/ab5ff3.

[24] A. Deb, A. Debnath, K. Bhowmik, S. Rudra Paul, B. Saha, Application of polyaniline impregnated mixed phase Fe_2O_3, $MnFe_2O_4$ and ZrO_2 nanocomposite for rapid abatement of binary dyes from aqua matrix: response surface optimisation, Int. J. Environ. Anal. Chem., (2021), doi: 10.1080/03067319.2021.1946683.

[25] A. Deb, A. Debnath, N. Bhattacharjee, B. Saha, Ultrasonically enhanced dye removal using conducting polymer functionalised ZnO nanocomposite at near neutral pH: kinetic study, isotherm modelling and adsorbent cost analysis, Int. J. Environ. Anal. Chem., (2020), doi: 10.1080/03067319.2020.1843649.

[26] T. Tripathy, R.P. Singh, Characterization of polyacrylamide-grafted sodium alginate: a novel polymeric flocculant, J. Appl. Polym. Sci., 81 (2001) 3296–3308.

[27] H. Zheng, J. Ma, F. Ji, X. Tang, W. Chen, J. Zhu, Y. Liao, M. Tan, Synthesis and application of anionic polyacrylamide in water treatment, Asian J. Chem., 25 (2013) 7071–7074.

[28] M.R. Manafi, P. Manafi, S. Agarwal, A.K. Bharti, M. Asif, V.K. Gupta, Synthesis of nanocomposites from polyacrylamide and graphene oxide: application as flocculants for water purification, J. Colloid Interface Sci., 490 (2017) 505–510.

[29] Y.Q. Wang, J. Pan, Y.H. Li, P.F. Zhang, M.X. Li, H. Zheng, X.P. Zhang, H. Li, Q.J. Du, Methylene blue adsorption by activated carbon, nickel alginate/activated carbon aerogel, and nickel alginate/graphene oxide aerogel: a comparison study, J. Mater. Res. Technol.-JMRT, 9 (2020) 12443–12460.

[30] M.F. Cui, Y.H. Li, Y. Sun, H.M. Wang, M.X. Li, L.B. Li, W.S. Xu, Degradation of tetracycline in polluted wastewater by persulfate over copper alginate/graphene oxide composites, J. Polym. Environ., 29 (2021), doi: 10.1007/s10924-020-02038-6.

[31] L.B. Li, Y.H. Li, K. Yang, X.Y. Luan, M.X. Li, M.F. Cui, Y. Sun, H.M. Wang, Q.Y. Sun, K.L. Tang, W.S. Xu, H. Zheng, Removal of Methylene blue from water by peach gum based composite aerogels, J. Polym. Environ., 29 (2021) 1752–1762.

[32] W. Zhao, Y. Fan, H. Wang, Y. Wang, Coacervate of polyacrylamide and cationic gemini surfactant for the extraction of methyl orange from aqueous solution, Langmuir, 33 (2017) 6846–6856.

[33] X. Yang, K. Chen, Y. Zhang, H. Liu, W. Chen, J. Yao, Polyacrylamide grafted cellulose as an eco-friendly flocculant: efficient removal of organic dye from aqueous solution, Fibers Polym., 18 (2017) 1652–1659.

[34] N. Kumar, H. Mittal, V. Parashar, S.S. Ray, J.C. Ngila, Efficient removal of rhodamine 6G dye from aqueous solution using nickel sulphide incorporated polyacrylamide grafted gum karaya bionanocomposite hydrogel, RSC Adv., 6 (2016) 21929–21939.

[35] M.A. Corona-Rivera, V.M. Ovando-Medina, L.A. Bernal-Jacome, E. Cervantes-Gonzalez, I.D. Antonio-Carmona, N.E. Davila-Guzman, Remazol red dye removal using poly(acrylamide-co-acrylic acid) hydrogels and water absorbency studies, Colloid Polym. Sci., 295 (2017) 227–236.

[36] L. Aref, A.H. Navarchian, D. Dadkhah, Adsorption of Crystal violet dye from aqueous solution by poly(acrylamide-co-maleic acid)/montmorillonite nanocomposite, J. Polym. Environ., 25 (2017) 628–639.

[37] G. Ma, Y. Shen, X. Wang, X. Guo, Z. Wu, Vermiculite/ polyacrylamide copolymers microspheres for profile control in oilfields, J. Appl. Polym. Sci., 134 (2017), doi: 10.1002/app.44918.

[38] L. Garcia-Uriostegui, G. Pineda-Torres, S. Lopez-Ramirez, J. Barragan-Aroche, C. Duran-Valencia, Inverse emulsion free-radical polymerization of acrylamide terpolymer for enhanced oil recovery application in harsh reservoir conditions, Polym. Eng. Sci., 57 (2017) 1214–1223.

[39] L.B. Li, Y.H. Li, K. Yang, M.X. Li, X.Y. Luan, Y. Sun, H.M. Wang, Q.Y. Sun, K.L. Tang, H. Zheng, M.F. Cui, W.S. Xu, Adsorption of methylene blue by *Nicandra physaloides* (L.) *gaertn* seed gum/graphene oxide aerogel, Environ. Technol., 10 (2021), doi: 10.1080/09593330.2021.1877361.

[40] Z.Q. Wang, G.H. Zhang, Y.H. Li, Preparation of chitosan/ polyacrylamide/graphene oxide composite membranes and study of their methylene blue adsorption properties, Materials, 13 (2020) 4407, doi: 10.3390/ma13194407.

[41] Y.L. Li, Y.H. Li, H.L. Zang, L. Chen, Z.H. Meng, H. Li, L.J. Ci, Q.J. Du, D.C. Wang, C.P. Wang, H.L. Li, Y.Z. Xia, $ZnCl_2$-activated carbon from soybean dregs as a high efficiency adsorbent for cationic dye removal: isotherm, kinetic, and thermodynamic studies, Environ. Technol., 41 (2020) 2013–2023.

[42] P. Das, A. Debnath, Reactive orange 12 dye adsorption onto magnetically separable $CaFe_2O_4$ nanoparticles synthesized by simple chemical route: kinetic, isotherm and neural network modeling, Water Pract. Technol., 16 (2021) 1141–1158.

[43] A. Deb, A. Debnath, B. Saha, Sono-assisted enhanced adsorption of eriochrome Black-T dye onto a novel polymeric nanocomposite: kinetic, isotherm, and response surface methodology optimization, J. Dispersion Sci. Technol., 42 (2021) 1579–1592.

[44] Q. Li, Y. Li, X. Ma, Q. Du, K. Sui, D. Wang, C. Wang, H. Li, Y. Xia, Filtration and adsorption properties of porous calcium alginate membrane for methylene blue removal from water, Chem. Eng. J., 316 (2017) 623–630.

[45] N.V. Farinella, G.D. Matos, M.A.Z. Arruda, Grape bagasse as a potential biosorbent of metals in effluent treatments, Bioresour. Technol., 98 (2007) 1940–1946.

[46] Z. Zhang, Y. Li, Q. Du, Q. Li, Adsorption of Congo red from aqueous solutions by porous soybean curd xerogels, Pol. J. Chem. Technol., 20 (2018) 95–102.

[47] Q. Du, J. Sun, Y. Li, X. Yang, X. Wang, Z. Wang, L. Xia, Highly enhanced adsorption of Congo red onto graphene oxide/ chitosan fibers by wet-chemical etching off silica nanoparticles, Chem. Eng. J., 245 (2014) 99–106.

[48] A.F. Hassan, A.M. Abdel-Mohsen, M.M.G. Fouda, Comparative study of calcium alginate, activated carbon, and their composite beads on methylene blue adsorption, Carbohydr. Polym., 102 (2014) 192–198.

[49] R. Bhattacharyya, S.K. Ray, Micro- and nano-sized bentonite filled composite superabsorbents of chitosan and acrylic copolymer for removal of synthetic dyes from water, Appl. Clay Sci., 101 (2014) 510–520.

[50] M.C.S. Reddy, L. Sivaramakrishna, A.V. Reddy, The use of an agricultural waste material, Jujuba seeds for the removal of anionic dye (Congo red) from aqueous medium, J. Hazard. Mater., 203 (2012) 118–127.

[51] M.K. Purkait, A. Maiti, S. DasGupta, S. De, Removal of Congo red using activated carbon and its regeneration, J. Hazard. Mater., 145 (2007) 287–295.

[52] B.H. Hameed, A.A. Ahmad, N. Aziz, Isotherms, kinetics and thermodynamics of acid dye adsorption on activated palm ash, Chem. Eng. J., 133 (2007) 195–203.

[53] M.H. Mahmoudian, M. Fazlzadeh, M.H. Niari, A. Azari, E.C. Lima, A novel silica supported chitosan/glutaraldehyde as an efficient sorbent in solid phase extraction coupling with HPLC for the determination of Penicillin G from water and wastewater samples, Arabian J. Chem., 13 (2020) 7147–7159.

[54] X. Yan, X. Zhang, Q. Li, Preparation and characterization of CS/ beta-CD/Nano-ZnO composite porous membrane optimized by Box–Behnken for the adsorption of Congo red, Environ. Sci. Pollut. Res., 25 (2018) 22244–22258.

[55] Y. Rashtbari, S. Hazrati, A. Azari, S. Afshin, M. Fazlzadeh, M. Vosoughi, A novel, eco-friendly and green synthesis of PPAC-ZnO and PPAC-nZVI nanocomposite using pomegranate peel: cephalexin adsorption experiments, mechanisms, isotherms and kinetics, Adv. Powder Technol., 31 (2020) 1612–1623.

[56] E. Bulut, M. Oezacar, I.A. Sengil, Equilibrium and kinetic data and process design for adsorption of Congo red onto bentonite, J. Hazard. Mater., 154 (2008) 613–622.

[57] V.K. Gupta, D. Pathania, S. Sharma, S. Agarwal, P. Singh, Remediation and recovery of methyl orange from aqueous solution onto acrylic acid grafted *Ficus carica* fiber: isotherms, kinetics and thermodynamics, J. Mol. Liq., 177 (2013) 325–334.

[58] R. Nodehi, H. Shayesteh, A.R. Kelishami, Enhanced adsorption of Congo red using cationic surfactant functionalized zeolite particles, Microchem. J., 153 (2020) 104281, doi: 10.1016/j. microc.2019.104281.

[59] K. Yang, Y. Li, H. Zheng, X. Luan, H. Li, Y. Wang, Q. Du, K. Sui, H. Li, Y. Xia, Adsorption of Congo red with hydrothermal treated shiitake mushroom, Mater. Res. Express, 7 (2020) 015103, doi: 10.1088/2053-1591/ab5ff3.

[60] H. Zhang, J. Zhou, Y. Muhammad, R. Tang, K. Liu, Y. Zhu, Z. Tong, Citric acid modified bentonite for Congo red adsorption, Front. Mater., 6 (2019), doi: 10.3389/fmats.2019.00005.

[61] M. Cui, Y. Li, Y. Sun, H. Wang, M. Li, L. Li, W. Xu, Study on adsorption performance of MgO/calcium alginate composite for Congo red in wastewater, J. Polym. Environ., 29 (2021) 3977–3987.

[62] S. Parvin, B.K. Biswas, M.A. Rahman, M.H. Rahman, M.S. Anik, M.R. Uddin, Study on adsorption of Congo red onto chemically modified egg shell membrane, Chemosphere, 236 (2019) 124326, doi: 10.1016/j.chemosphere.2019.07.057.

[63] S. Al-Salihi, A.M. Jasim, M.M. Fidalgo, Y. Xing, Removal of Congo red dyes from aqueous solutions by porous γ-alumina nanoshells, Chemosphere, 286 (2022) 131769, doi: 10.1016/j. chemosphere.2021.131769.

[64] A. Azari, R. Nabizadeh, A.H. Mahvi, S. Nasseri, Integrated Fuzzy AHP-TOPSIS for selecting the best color removal process using carbon-based adsorbent materials: multi-criteria decision making vs. systematic review approaches and modeling of textile wastewater treatment in real conditions, Int. J. Environ. Anal. Chem., (2020), doi: 10.1080/03067319.2020.1828395.

[65] N. Yeddou, A. Bensmaili, Kinetic models for the sorption of dye from aqueous solution by clay-wood sawdust mixture, Desalination, 185 (2005) 499–508.

[66] O. Duman, E. Ayranci, Adsorptive removal of cationic surfactants from aqueous solutions onto high-area activated carbon cloth monitored by in situ UV spectroscopy, J. Hazard. Mater., 174 (2010) 359–367.

[67] J. Zhou, P. Wu, Z. Dang, N. Zhu, P. Li, J. Wu, X. Wang, Polymeric Fe/Zr pillared montmorillonite for the removal of Cr(VI) from aqueous solutions, Chem. Eng. J., 162 (2010) 1035–1044.

[68] A. Azari, M. Yeganeh, M. Gholami, M. Salari, The superior adsorption capacity of 2,4-dinitrophenol under ultrasound-assisted magnetic adsorption system: modeling and process optimization by central composite design, J. Hazard. Mater., 418 (2021) 126348, doi: 10.1016/j.jhazmat.2021.126348.